

# Early stages of tin bronze corrosion in neutral aqueous chloride media: Electrochemical and FTIR investigations

S. Aouadi and N. Souissi\*

The corrosion behavior of tin bronze alloy equivalent to a Punic one was investigated in aqueous 0.5 M chloride electrolyte using potentiodynamic measurements. The electrochemical results showed selective dissolution of the major alloy component reflecting a decuprification process. FTIR characterization of the patina anodic layers showed the presence of various dehydrated and hydrated tin compounds with a few copper species suggesting the patina type I formation on the Cu<sub>10</sub>Sn bronze alloy. A kinetic model for the Cu<sub>10</sub>Sn bronze alloy dissolution in the chloride solution was developed. The reaction order with respect to chloride content was determined for the Cl<sup>-</sup> halide concentration domains. The low order value (about 0.22) was attributed to the Cl<sup>-</sup> adsorption intermediate step. The high reaction order value (about 2) reflected two determining steps of cuprous chloride complex formation. Two behaviors for the material were evidenced when varying the temperature. The values of the activation energy  $E_a$ , activation enthalpy  $\Delta H^*$  and activation entropy  $\Delta S^*$  were calculated and discussed.

## 1 Introduction

Preserving our bronze cultural heritage requires the investigation of copper tin alloys corrosion behavior in various burying media.

Materials alteration phenomena in chloride containing electrolytes have attracted many research programs [1–3] as the ambiguous halide effect on the corrosion morphology type (Cl<sup>-</sup> was assumed leading to type II but type I could be encountered [4]). We used the cyclic voltammetry technique to explore the electrochemical behavior of Punic bronze in chloride electrolyte [5]. The formation of compact patina layer grown on the bronze surface was evidenced which was different from pure metals. We studied also modern and archaeological bronze corrosion behaviors in chloride media [6]. Results obtained allowed us concluding that although the differences between both materials quite similarities were evidenced in their electrochemical behaviors. Indeed, the copper tin alloys were evidenced exhibiting two types of electrochemical responses when halide content varied. *Robbiola* et al. [7] investigated the

Cu<sub>10</sub>Sn corrosion behavior in aqueous chloride electrolyte. The authors stated that 0.1 M chloride medium could enhance type I corrosion morphology.

However, to the best of our knowledge there was no investigations on the kinetics of the corrosion process evolved (transformation order vs. the halide environment content and thermodynamics parameters of the activation reaction).

The aim of present research program was to study the early stages of corrosion of tin bronze alloy in neutral aqueous chloride media. Stationary electrochemical technique was used in order to investigate the effects of electrolyte halide content, immersion time in the chloride electrolyte and temperature on the material corrosion behavior. FTIR was employed to characterize the anodic formed patina layers.

## 2 Experimental

The electrochemical experiments were carried out in a classical three-electrode cell: a platinum wire as counter electrode, a bronze-disk as working electrode and a calomel electrode in saturated KCl solution (SCE) as reference. The working electrode was prepared of a Cu<sub>10</sub>Sn bronze alloy (active area 0.3 cm<sup>2</sup>). The bronze was elaborated as described above [8]. The material was embedded in a chemically inert resin and mechanically polished up to 4000 SiC grade before use. The measurements were done in a stagnant, aerated neutral chloride solution (0.5 M NaCl). The experiments were conducted on a Voltalab 10. Voltmaster

S. Aouadi, N. Souissi

University of Tunis El Manar, Institut Préparatoire aux Etudes d'Ingénieurs d'El Manar, BP 244 El Manar II, 2092, El Manar (Tunisia)  
E-mail: nebil.souissi@utm.rnu.tn, nebilSouissi@gmail.com

S. Aouadi

University of Carthage, Faculté des Sciences de Bizerte, 7021, Zarzouna (Tunisia)

software was used for instrumentation control and data treatments. The potentiodynamic measurements started at the open circuit potential ( $E_{ocp}$ ) reached after 5 min of immersion in the corrosive electrolyte. The anodic domain ranged from  $E_{ocp}$  to 1 V whereas the cathodic interval was from  $E_{ocp}$  to  $-2$  V. The scan rate was fixed at 10 mV/s. The influence of temperature on the corrosion behavior of the alloy was evaluated in the range 300–323 K. All experiments have been replicated at least three times. The material surface was analyzed by Fourier transform infrared spectrometry using a Nicolet 200 FTIR spectrometer.

### 3 Results and discussion

#### 3.1 Morphology of the polarization curves

The polarization curves of Cu10Sn electrode were performed after 5 min of immersion in 0.5 M NaCl solution. Figure 1 gathered the cathodic and anodic obtained curves.

The cathodic curve for bronze immersed in chloride electrolyte exhibited three successive domains (Fig. 1a). The first from  $-2$  to  $-1.35$  V/SCE was attributed to water evolution. The second domain from  $-0.8$  to 1.35 V/SCE was assigned to a plateau of oxygen diffusion and the current limit ( $J_L$ ) was about 1.7 mA/cm<sup>2</sup>. Finally, the domain located at  $-0.8$  V/SCE  $- E_{ocp}$  was characterized by a charge transfer-reduction of surface

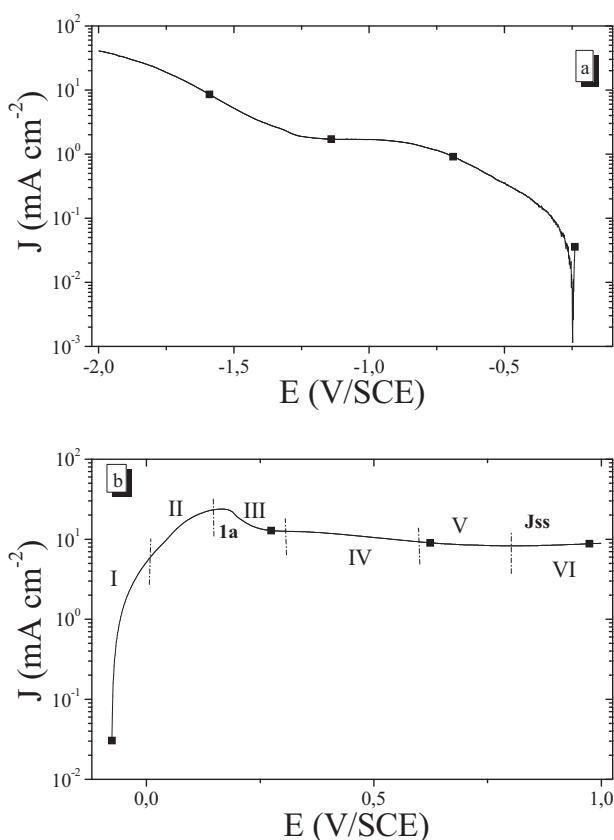


**Figure 1.** Polarization curves of bronze immersed in 0.5 M sodium chloride electrolyte; cathodic range (a), anodic range (b)

species. It corresponded to the cathodic interval of the Tafel domain.

The anodic curve is presented in Fig. 1b. The first domain corresponded to the anodic part of Tafel behavior. The wide anodic peak (1a) appeared at 0.167 V/SCE with a maximum at 24 mA/cm<sup>2</sup> corresponding to the simultaneous oxidation of tin and copper species [6,7]. At more positive potentials, the current density decreased and a current plateau occurred which could be assigned to the formation of the corrosion products containing tin hydroxychloride and cuprous chloride [6,7]. The steady state current ( $J_{ss}$ ) was about 8.8 mA/cm<sup>2</sup> at 1 V/SCE.

The evolution of corrosion layers at different potential intervals marked from I to VI were characterized using FTIR. The FTIR spectra were recorded in the wavenumber range 400–4000/cm. Figure 2 depicts the obtained spectra.

It is worth noting that the peaks detected in the region 2000–2800/cm were not considered. The spectra show a clear difference. For example, in region I the bands were poorly resolved. A broad band at 3425/cm could be assigned to the hydroxyl vibration stretching. The band centered at 1647/cm was due to the in plane OH deformation and the weak bands in the 700–400/cm range were attributed to the Sn(IV)–O, Sn(II)–O, and Sn–OH stretching vibrations [9–12]. For region II, bands at 3478.6 and 3360/cm were more resolved indicating the presence of different type of OH group. This was confirmed by the intense band at 753/cm which was assigned to different oxygen-bridged tin species [9]. The weak band at 1609/cm was related to the H–O–H deformation [7]. On the other hand, the peak occurring at 683/cm was characteristic of SnO<sub>2</sub> stretching mode, while the peaks at 508 and 428/cm could correspond to Sn–O and Sn–Cl bending vibrations, respectively [13]. Increasing the anodic potential (region III), an increase in the hydroxyl intensity band was observed at 3408 (stretching vibration) and 1647/cm (OH deformation). Furthermore, one can note the appearance of peaks at 1247 and 1148/cm: the first was due to OH bending in Sn(OH)<sub>2</sub>, while the second was assigned to the overtones of Sn–OH. The shoulder in the wavenumber range 400–800/cm could be due to Sn–O–Sn and Sn–OH stretching mode [7,9]. In

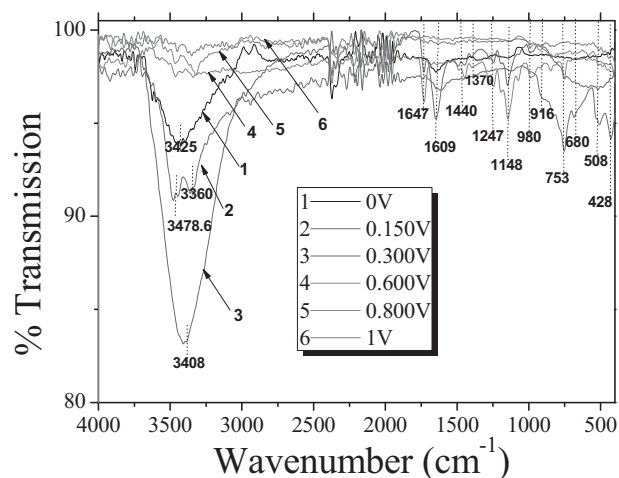


**Figure 2.** FTIR spectra of corrosion layer grown on the Cu10Sn electrode during anodic polarization

the region IV, peaks at the low wavenumber region were more resolved but the intensity of OH stretching band decreased and the OH deformation of water shifted to 1740/cm. Bands in the range 1370–1440/cm may be attributed to the overtones of the Sn–O–Sn [7,10]. The bands located at 980 and 916/cm could be assigned to the OH deformation of tin hydroxychloride as well as the presence of a few copper hydroxychloride [7,14]. In the passive domain (V and VI), the peaks intensity markedly decreased with increase in anodic potential. Therefore, it could be concluded that main corrosion products were tin-enriched layer (dehydrated and hydroxychloride tin species) and a few copper compounds which could reflect the type I patina formation on the Cu10Sn bronze alloy.

From the Tafel domain, the extrapolation of linear line to corrosion potential ( $E_{corr}$ ) gives a straight line and the slope gives both  $\beta a$  and  $\beta c$ , and the intercept gives the corrosion current ( $J_{corr}$ ). Furthermore, Tafel slopes extrapolations were used to determine the proportionality factor ( $B$ ). The polarization resistance ( $R_p$ ) was calculated by means of the Stern-Geary relationship (Equation (1)) [15]:

$$R_p = \frac{\beta a \beta c}{2.3(\beta a + \beta c) J_{corr}} = \frac{B}{J_{corr}} \quad (1)$$

The corresponding electrochemical parameters are listed in Table 1.

After 5 min of immersion in the chloride electrolyte the corrosion potential was  $-0.160$  V/SCE. Such a value was close to those found for Cu10Sn alloy [6] and archeological bronze [16] immersed at extended time in aqueous chloride electrolyte ( $-0.152$  and  $-0.170$  V/SCE, respectively). However,  $E_{corr}$  was more anodic than those obtained for Cu–Sn alloys including Pb, Ni, and Zn alloying immersed for longer times in chloride electrolyte [17–19]. The difference in  $E_{corr}$  could be explained by the differences of the experimental conditions as well as the materials compositions and microstructures.

The anodic Tafel slope  $\beta a$  was found to be 64 mV/dec. This value is generally observed for pure copper and copper based alloy immersed in aerated aqueous chloride medium (about 60 mV/dec) [20,21]. It denoted the selective copper dissolution for the Cu10Sn bronze alloy according to the following reaction (Equation (2)):



However,  $\beta a$  values in the range 24–28 mV/dec were also reported [17,19]. The difference in the anodic Tafel slopes could be related to the difference in the charge transfer coefficient, so

dissolution mechanism process changed for the different bronzes.

The cathodic Tafel slope was about  $-258$  mV/dec, which is consistent with  $\beta c$  determined for copper based alloy freshly immersed in 3.0–3.5% w/w NaCl [20]. It could reflect the exchange of four electrons in the oxygen reduction reaction (Equation 3):



The cathodic Tafel slope was higher compared to the literature results [17–19], which could indicate different electron exchange in the cathodic reaction.

The proportionality factor  $B$  was about 22 mV which was higher than those obtained for the alloying bronzes. But, it remained in the range observed in the literature for copper based materials (5–31 mV) [20].

The corrosion current density  $J_{corr}$  and the polarization resistance  $R_p$  were  $26 \mu\text{A}/\text{cm}^2$  and  $852 \Omega/\text{cm}^2$ , respectively. These values were higher than those found in the literature data [17–19] which could be explained notably in terms of experimental conditions but also by the corrosion mechanisms evolved. In fact, our material alteration phenomenon seems to be mostly affected by the major alloy components (Cu). So, material decuprification could be announced at the early stages of Cu10Sn corrosion.

### 3.2 Effect of the immersion time in aqueous chloride electrolyte

In order to study the immersion time effect on the material electrochemical behavior, the Cu10Sn bronze alloy was immersed in the 0.5 M NaCl chloride electrolyte for various exposure times (5, 15, 30, and 60 min). Figure 3 shows the anodic and cathodic obtained curves.

Independently on the immersion time, we noticed that the cathodic current decreased when time increased (Fig. 3a). Furthermore, the global curve shape does not change as three domains were also evidenced. However, a cathodic activation peak was clearly shown for 60 min. Its potential and current density were  $-1$  V/SCE and  $3.1 \text{ mA}/\text{cm}^2$ , respectively. It could be attributed to tin species reduction [6]. However, For long immersion times ( $>20$  h) Ammelot et al. ascribed the cathodic peak of Cu13Sn to the simultaneous reduction of  $\text{Cu}_2\text{O}$  and  $\text{Sn}_2\text{O}$  [3].

The global shape of the bronze anodic curve was not changed when the immersion time increased (Fig. 3b). In fact three potential domains were also noticed. However,  $J_{SS}$  tended

**Table 1.** Electrochemical parameters obtained from polarization curves

Ref	Immersion time (min)	$E_{corr}$ (V/SCE)	$\beta a$ (mV/dec)	$-\beta c$ (mV/dec)	$B$ (mV)	$J_{corr}$ ( $\mu\text{A}/\text{cm}^2$ )	$R_p$ ( $\Omega/\text{cm}^2$ )
Our work	5	$-0.160$	64	258	22	26	852
[17]	60	$-0.298$	24.9	9.28	3	7.35	403
[18]	60	$-0.215$	–	6.89	–	9.88	–
[19]	60	$-0.210$	27.02	22.22	5	11.97	443

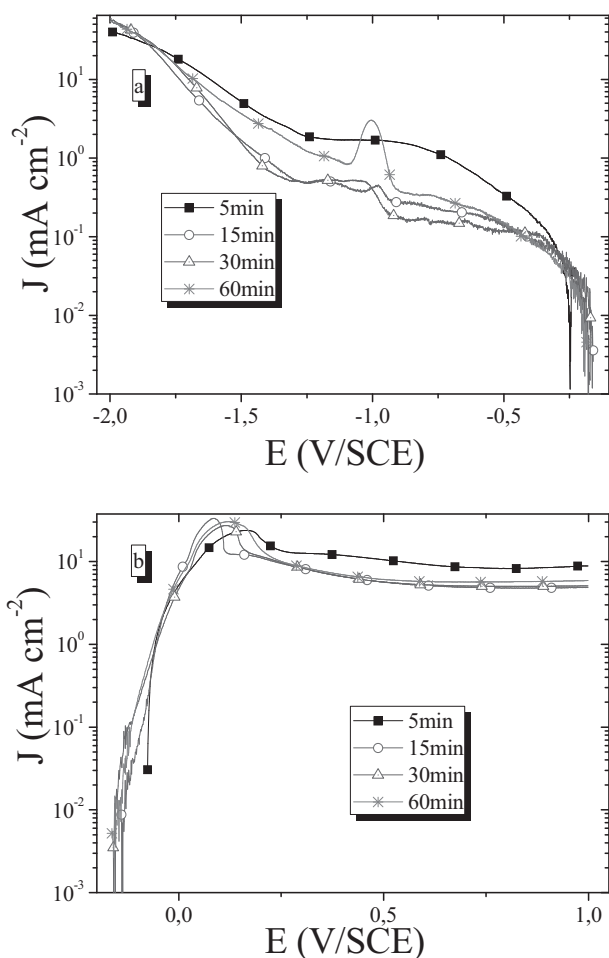


**Figure 3.** Effect of the immersion time in chloride solution on the electrochemical behavior of Cu10Sn alloy; cathodic branch (a) anodic branch (b)

rapidly to a constant value of about  $8.2 \text{ mA/cm}^2$  at  $E = 1 \text{ V/SCE}$  for immersion times up to 15 min.

The electrochemical parameters obtained in the Tafel region are summarized in Table 2.

It was found that the corrosion potential tended to cathodic values indicating the increase of the material surface reactivity. The anodic Tafel slope was not affected by the increase of the immersion time. Hence, the oxidation reaction was not changed. A second Tafel slope ( $\beta a^{\text{ps}}$ ) was determined in the vicinity of the anodic peak as *Neodo* et al. [21] and the results are listed in Table 2. Independently on the immersion time, the pseudo-Tafel slope was about  $210 \text{ mV/dec}$ , which was

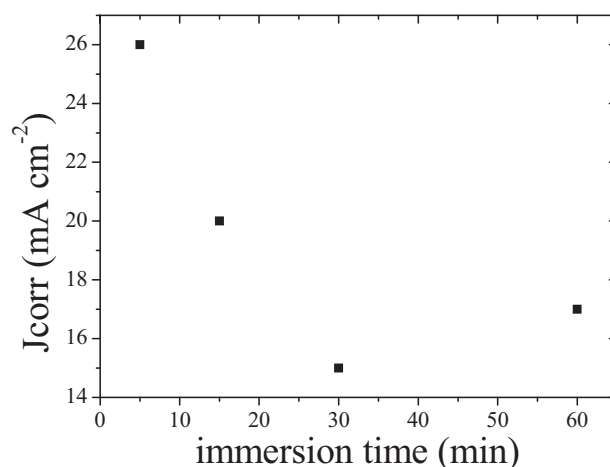


**Figure 4.** Evolution of the corrosion current density variation with the immersion time in the chloride electrolyte

related to the chemical transformation of  $\text{CuCl}$  into  $\text{CuCl}_2^-$  (Equation (4)) [21]:



As to the cathodic Tafel slope values, they decreased slightly to reach  $208 \text{ mV/dec}$  after 30 min. Such a result could be linked to the change of the electron exchange in the cathodic reaction by the reduction of the corrosion products.

The proportionality factor kept almost the same values increasing the immersion time.

In order to study the evolution of the corrosion current density, the  $J_{\text{corr}}$  variation was plotted with the immersion time in the chloride electrolyte (Fig. 4).

It was found that the corrosion current density decreased progressively to reach  $15 \mu\text{A/cm}^2$  after 30 min, reflecting a decrease in the corrosion rate. Inversely, the polarization resistance increased from  $852$  to  $1325 \Omega/\text{cm}^2$  with the contact in the chloride electrolyte.

So the decrease in the corrosion rate may be explained in terms of the development of a noble patina layer at the Cu10Sn bronze alloy which narrowed the corrosion process.

### 3.3 The effect of chloride concentration

The influence of the chloride concentration on the corrosion behavior of Cu10Sn alloy was also investigated. Figure 5 depicts the obtained curves for different chloride contents ranging from 0.1 to 1 M.

**Table 2.** Corrosion parameters at different Cu10Sn alloy immersion time in the chloride solution

Time (min)	$E_{\text{corr}}$ (V/SCE)	$\beta a^{\text{app}}$ (mV/dec)	$\beta a^{\text{ps}}$ (mV/dec)	$-\beta c$ (mV/dec)	$B$ (mV)	$J_{\text{corr}}$ ( $\mu\text{A/cm}^2$ )	$R_p$ ( $\Omega/\text{cm}^2$ )
5	-0.160	64	211	258	22	26	852
15	-0.158	59	209	252	21	20	1039
30	-0.172	65	210	208	21	15	1440
60	-0.178	64	210	273	22	17	1325

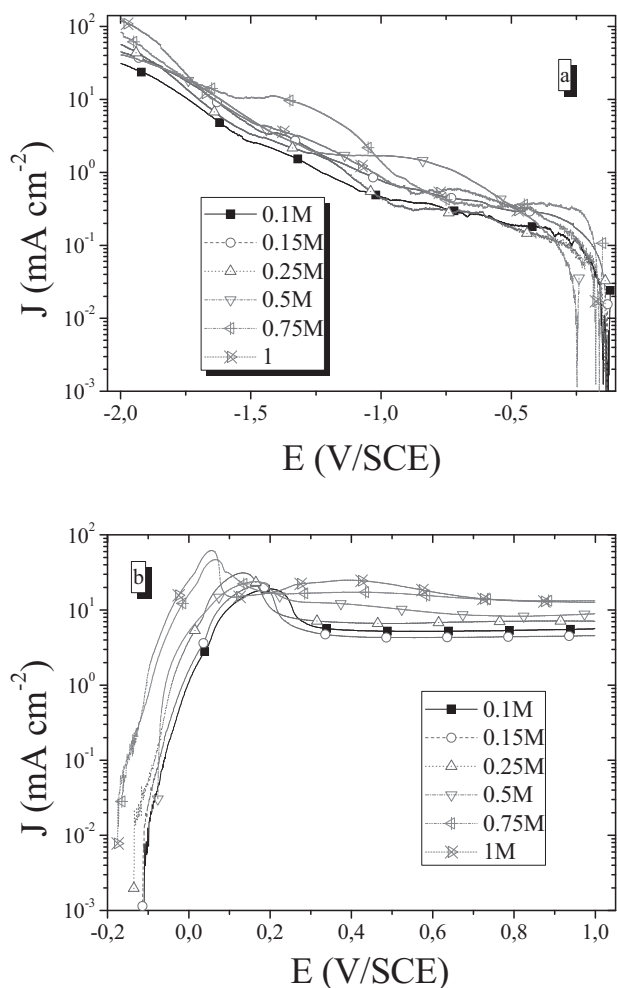


**Figure 5.** Cathodic (a) and anodic (b) polarization curves for Cu10Sn alloy in different chloride solutions

As presented in Fig. 5a, the shape of the cathodic curves exhibited globally similar trend, except the decrease of the oxygen diffusion plateau with the reduced chloride concentrations. As can be seen from Fig. 5b, the increase of chloride ions led to an increase in the current density of the anodic peak and to a shift to the cathodic region. Thus the electrode was more active with halide addition.

The electrochemical parameters extracted from the J-E curves are listed in Table 3.

**Table 3.** Kinetics parameters obtained with different halide concentration

$[Cl^-]$ (mol/L)	$E_{corr}$ (V/SCE)	$\beta_a$ (mV/dec)	$-\beta_c$ (mV/dec)	$B$ (mV)	$J_{corr}$ ( $\mu A/cm^2$ )	$R_p$ ( $\Omega/cm^2$ )
0.10	-0.115	64	162	20	18.03	1104
0.15	-0.120	61	85	15	20.02	766
0.25	-0.145	61	200	20	22.30	914
0.50	-0.160	64	258	22	26	852
0.75	-0.165	61	109	17	77.8	219
1	-0.180	67	478	26	102.3	250

It was found that the corrosion potential was more positive at lower chloride concentration. The anodic Tafel slope was as usual 60 mV/dec ( $\pm 4$ ). However the cathodic Tafel slope changed with the decrease in halide concentration. Concerning the corrosion current density, it increased by rising chloride contents. This indicates an enhanced corrosion rate with the increase of aggressive medium.

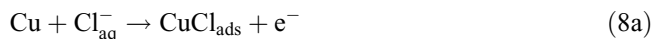
In order to elucidate the corrosion mechanism of the Cu10Sn bronze alloy in neutral chloride solution, the reaction order with respect to  $Cl^-$  ions was determined. Thus, the corrosion current density can be expressed according to equation (5) [21]:

$$J_{corr} = [Fk_4(k_2/k_{-2})[Cl^-]^\alpha / (1 + k_{-4})t / m_{CuCl_2}] e^{(\frac{FE}{2.3RT})} \quad (5)$$

Where,  $F$  is the Faraday constant,  $t$  is the total surface site concentration,  $\alpha$  is the reaction order with respect to the chloride ions,  $m_{CuCl_2}$  is the ratio between the  $CuCl_2^-$  diffusion coefficient and the diffusion thickness layer,  $k_2$  and  $k_4$  are the rate constants of reaction (2) and (4).

Figure 6 shows the trend of  $\log J_{corr}$  with respect to the  $\log [Cl^-]$ . Two behaviors were evidenced when varying the chloride ions content.

In the first domain ( $0.1 M < [Cl^-] < 0.5 M$ ) the reaction order was about 0.22. The obtained reaction order was lower than that found for Ni-Al-bronze [21] and pure copper [22]. A very low reaction order (0.16) was found for iron dissolution in sulphate medium in a wide concentration range 0.0001–0.075 M [23]. Such reaction order was explained by an adsorption of the sulphate ions as an intermediate step. It could be concluded that the very low reaction order could indicate the Cu10Sn bronze alloy corrosion was not notably dependent on  $Cl^-$  ions. The last may act as a corrosion reaction initiator. So the  $Cl^-$  ions adsorption may be an intermediate step and the formed  $CuCl$  complex could be dissociated. The Cu10Sn bronze alloy dissolution may follow the following reactions (Equations 6–9):



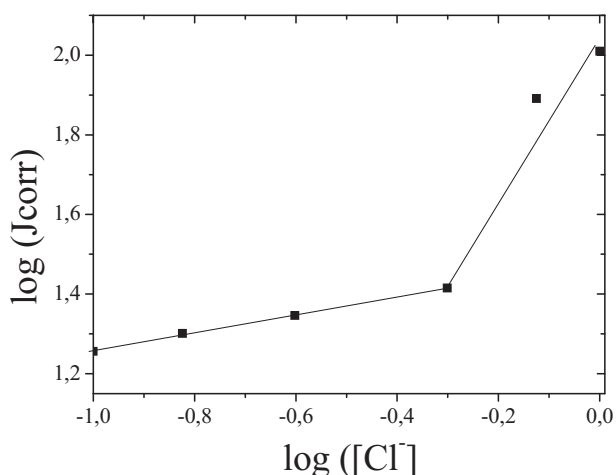
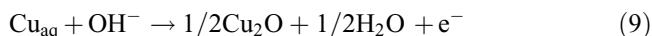


**Figure 6.** Cu<sub>10</sub>Sn alloy reaction order with respect to chloride content



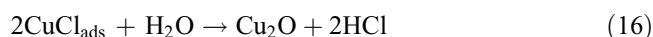
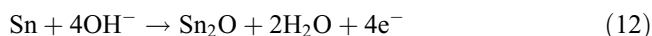
In the second interval ( $0.5 \text{ M} < [\text{Cl}^-] < 1 \text{ M}$ ), the reaction order was the usual 2 generally observed for copper based alloy in chloride medium. According to previous researches, the reaction order was about 2 for chloride concentration lower than 1 M [21,22]. The authors concluded that the oxidation of copper or copper alloy was considerably dependent on halide content. However when the chloride concentration exceeded 1 M, the reaction order was 2.4 and the highest value was attributed to the formation of substantial amounts of copper chloride species [21,22].

In addition, the dissolution mechanism of copper has been widely studied in chloride solution [21,24–25]. The model proposed by a number of authors consisted of two determining steps (Equations 10 and 11):



Furthermore, the presence of Cu<sub>2</sub>O was also evidenced on copper surface in chloride containing solutions [25–27].

For Cu<sub>10</sub>Sn alloy, the oxidation of the major component could be generally accompanied by the alloying element oxidation. As a result, an oxide layer of copper and tin oxihydroxides may grow at the bronze surface. Then the bronze substrate may undergo the following dissolution mechanism (Equations 12–16):



### 3.4 The influence of temperature

The influence of temperature on the kinetic process of bronze corrosion was also evaluated. The polarization curves were plotted after 5 min of immersion in the chloride electrolyte at various temperatures ranging from 300 to 323 K. Figure 7 illustrates the obtained curves.

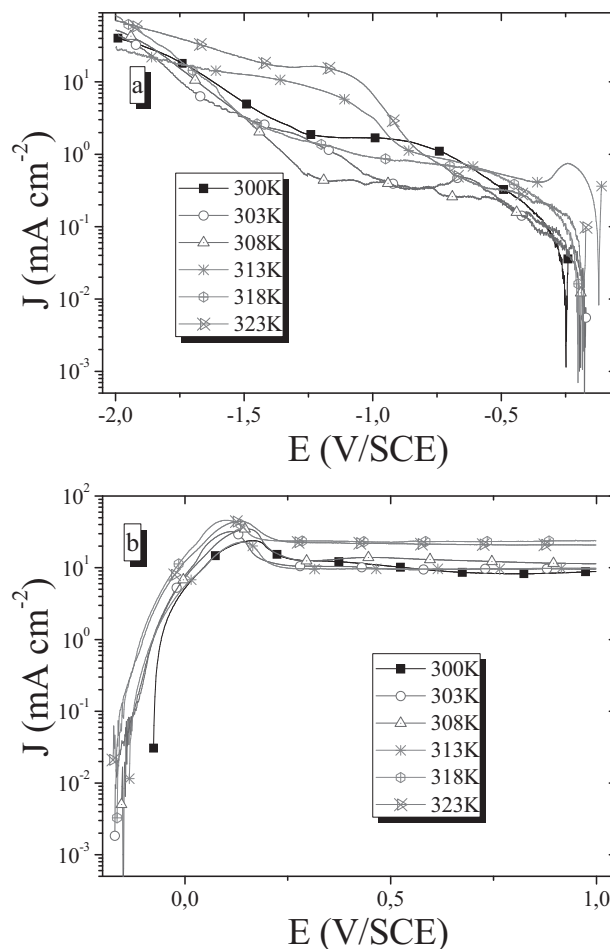


**Figure 7.** Cathodic (a) and anodic (b) polarization curves obtained in 0.5 M NaCl at various temperatures

**Table 4.** Corrosion parameters of Cu10Sn electrode at different temperatures obtained from polarization curves

$T$ (K)	$E_{corr}$ (V/SCE)	$\beta a$ (mV/dec)	$-\beta c$ (mV/dec)	$B$ (mV)	$J_{corr}$ ( $\mu\text{A}/\text{cm}^2$ )	$R_p$ ( $\Omega/\text{cm}^2$ )
300	-0.160	64	258	22	26	852
303	-0.182	67	206	22	28	785
308	-0.178	66	275	23	27	850
313	-0.134	54	55	12	113	105
318	-0.225	108	491	38	133	288
323	-0.215	110	850	42	153	277

It appeared that the anodic and cathodic curves were modified by the increase in temperature.

As presented in Fig. 7a, the cathodic behavior showed an evolution. It could be mentioned that the current peaks which appeared in the potential range [ $E_{OCP}$ ;  $-0.8$  V/SCE] could correspond to copper species reduction. However, the large current peak occurring at the lower potential range could be linked to tin compounds reduction [6].

The anodic curves (Fig. 7b) showed a shift of the activation peak to the negative values and an increase of its current density.

From the extrapolated Tafel regions, the electrochemical parameters were determined. Table 4 depicts the various kinetics corrosion parameters.

The results clearly showed that the corrosion potential shifted to the cathodic range. It was reported in previous studies that an increase of temperature led to a change in the corrosion potentials for many substrates in different media [28–31]. The positive shift of  $E_{corr}$  was attributed to metal passivation. However, the shift in  $E_{corr}$  toward the cathodic value could be due to the increase in the material surface reactivity.

Nevertheless, the corrosion current density seems to be constant from 300 to 308 K. At higher temperatures,  $J_{corr}$  increased substantially which could be assigned to an acceleration of the corrosion rate. The anodic and cathodic Tafel slopes have almost constant values in the temperature range 300–308 K, suggesting that the corrosion mechanism was not affected by the increase of temperature. However, for higher temperatures a significant change of the Tafel slopes was observed.

The dependence of the corrosion current density on temperature can be expressed by the Arrhenius equation (Equations 17) [32]:

$$J_{corr} = A \exp\left(\frac{-Ea}{RT}\right) \quad (17)$$

where  $Ea$ : activation energy,  $R$ : universal gas constant;  $A$ : pre-exponential factor and  $T$ : absolute temperature.

The plot of  $\ln J_{corr}$  versus  $1/T$  gave a straight line in the last temperature range (Fig. 8). It is obvious that Arrhenius plot showed a break at around 313 K, thus the value of  $Ea$  was calculated in the temperature range 313–323 K and the results are gathered in Table 5.

For the first interval, the corrosion rate was not affected by temperature increase. The non-Arrhenius behavior was also observed for pure copper in a Tunisian soil [33] and in sodium bromide containing solution [34]. The authors have attributed

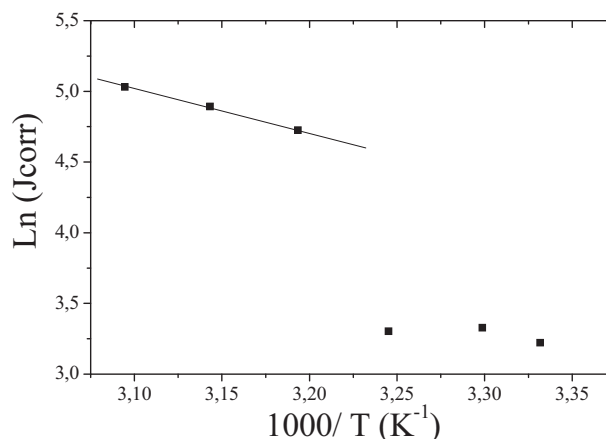
such observations to an increase of anion aggressiveness, which was counterbalanced by the growth of a thick oxide layer at elevated temperature [33,34].

In the last domain, the slope yielded apparent activation energy of 25.7 kJ/mol. Such values were higher than those obtained for Al-bronze in 3–3.5% NaCl solution (14.9 and 16.64 kJ/mol) [32,35].

Furthermore, the activation thermodynamic parameters  $\Delta H^*$  and  $\Delta S^*$  of the bronze corrosion reaction in the chloride electrolyte were calculated from the transition-state plot according to equation (18) [32]:

$$J_{corr} = \frac{RT}{Nh} \exp\left(\frac{\Delta S^*}{R}\right) \exp\left(\frac{-\Delta H^*}{RT}\right) \quad (18)$$

where  $R$ : universal gas constant;  $T$ : absolute temperature;  $N$ : Avogadro's number;  $h$ : Planck's constant;  $\Delta H^*$ : activation enthalpy;  $\Delta S^*$ : activation entropy.

**Figure 8.** Arrhenius plot for Cu10Sn electrode in chloride solution**Table 5.** Values of activation parameters ( $Ea$ ,  $\Delta H^*$ , and  $\Delta S^*$ ) for modern tin bronze

$T$ (K) 313–323		
$Ea$ (kJ/mol)	$\Delta H^*$ (kJ/mol)	$\Delta S^*$ (J/mol K)
25.7	22.4	-132.7

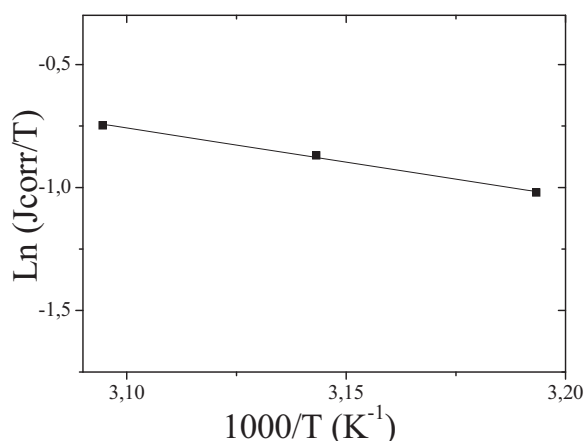


**Figure 9.** Transition-state plot for bronze immersed in 0.5 M NaCl medium

Figure 9 gives the transition-state plot obtained.

In the latter domain, the bronze corrosion rate fitted a transition-state plot with a slope and intercept yielding the activation enthalpy and entropy, respectively. The values of the activation parameters are given in Table 4. Analysis of Table 4 showed that the activation enthalpy  $\Delta H^*$  was of the order of 22.4 kJ/mol. Such a value was higher than those found for Al-bronze (8.9 kJ/mol) [32]. The positive value of  $\Delta H^*$  could reflect the endothermic nature of bronze dissolution.

Moreover, the activation entropy  $\Delta S^*$  has a negative value ( $-132.7$  J/mol K). This indicated that the activated complex in the rate determining step represented an association rather than dissociation, suggesting a decrease in disordering on going from reactants to activated molecules [32].

## 4 Conclusions

Electrochemical and FTIR investigations were carried out in order to study the early stages of tin bronze alloy corrosion in neutral aqueous chloride solution. The electrochemical results allowed us to conclude that the Cu<sub>10</sub>Sn bronze alloy oxidation proceeded from decuprification process. FTIR characterizations showed the presence of tin-enriched patina layer with few copper species. The reaction order with respect to chloride ions was determined in two concentration ranges. For  $[\text{Cl}^-] < 0.5$  M, the reaction order was about 0.22 suggesting that the Cu<sub>10</sub>Sn bronze alloy dissolution was not strongly dependent on  $\text{Cl}^-$  ions which could act as corrosion initiator. For  $[\text{Cl}^-] > 0.5$  M the bronze dissolution mechanism was controlled by copper oxidation. Two determining steps were evidenced where the cuprous chloride formation was followed by  $\text{CuCl}_2^-$  complex. With the rise of temperature two behaviors were found. For the first temperature range, the corrosion rate of bronze corrosion was relatively constant. In the later interval, the corrosion current density substantially increased and for the Cu<sub>10</sub>Sn bronze alloy corrosion an endothermic reaction was found.

**Acknowledgments:** The authors wish to thank Dr M.A.K. Sanhoury, MRSC, of the department of chemistry, Faculty of Sciences of Tunis for technical assistance.

## 5 References

- [1] S. I. Pyun, Y. G. Chun, *Brit. Corr. J.* **1996**, *31*, 147.
- [2] F. Ammelot, C. Fiaud, E. M. M. Sutter, *Electrochim. Acta.* **1999**, *44*, 2549.
- [3] C. Debiemme-Chouvy, F. Ammelot, E. M. M. Sutter, *App. Surf. Sci.* **2001**, *174*, 55.
- [4] N. Souissi, L. Bousselmi, S. Khosrof, E. Triki, *Mater. Corros.* **2004**, *4*, 55.
- [5] L. Robbiola, J. M. Blengino, C. Fiaud, *Corros. Sci.* **1998**, *40*, 2083.
- [6] N. Souissi, E. Sidot, L. Bousselmi, E. Triki, L. Robbiola, *Corros. Sci.* **2007**, *49*, 3333.
- [7] L. Robbiola, T. T. M. Tran, P. Dubot, O. Majerus, R. Rahmouni, *Corros. Sci.* **2008**, *50*, 2205.
- [8] E. Sidot, N. Souissi, L. Bousselmi, E. Triki, L. Robbiola, *Corros. Sci.* **2006**, *48*, 2241.
- [9] C. A. Moina, G.O Ybarra, *J. Electroanal. Chem.* **2001**, *504*, 175.
- [10] V. Brunetti, M. L. Teijelo, *J. Electroanal. Chem.* **2008**, *613*, 16.
- [11] A. S. Tselesh, *Thin. Solid. Film.* **2008**, *516*, 6253.
- [12] X. Zhong, G. Zhang, Y. Qiu, Z. Chen, X. Guo, C. Fu, *Corros. Sci.* **2013**, *66*, 14.
- [13] B. X. Huang, P. Tornatore, Y-S. Li, *Electrochim. Acta.* **2000**, *46*, 671.
- [14] S. Jouen, B. Lefez, M. T. Sougrati, B. Hannoyer, *Mater. Chem. Phys.* **2007**, *105*, 189.
- [15] L. Stern, A. L. Geary, *J. Electrochem. Soc.* **1957**, *104*, 56.
- [16] N. Souissi, L. Bousselmi, S. Khosrof, E. Triki, *Ann. Chim. Sci. Mat.* **2005**, *30*, 103.
- [17] A. Dermaj, N. Hajjaji, S. Joiret, R. Rahmouni, A. Srhiri, H. Takenouti, V. Vivier, *Electrochim. Acta.* **2007**, *52*, 4654.
- [18] D. Chebabe, A. Dermaj, H. Erramli, A. Hajjaji, *Anti-Corros. Meth. Mater.* **2014**, *6*, 281.
- [19] A. Dermaj, D. Chebabe, M. Doubi, H. Erramli, N. Hajjaji, M. P. Casaletto, G. M. Ingo, C. Riccurci, T. D. Caro, *Corros. Engineer. Sci. Tech.* **2015**, *50*, 128.
- [20] G. Kear, B. D. Barker, F. C. Walsh, *Corros. Sci.* **2004**, *46*, 109.
- [21] S. Neodo, D. Carugo, J. A. Wharton, K. R. Stokes, *J. Electroanal. Chem.* **2013**, *695*, 38.
- [22] H. P. Lee, K. Nobe, A. J. Pearlstein, *J. Electrochem. Soc.* **1986**, *133*, 1031.
- [23] KJ. Vetter, F. Gorn, *Electrochim. Acta.* **1973**, *18*, 321.
- [24] B. Yuan, C. Wang, L. Li, S. Chen, *Electrochem. Com.* **2009**, *11*, 1373.
- [25] S. M. Milic, M. M. Antonijevic, *Corros. Sci.* **2009**, *51*, 28.
- [26] G. D. Zhou, H. Shao, B. H. Loo, *J. Electroanal. Chem.* **1997**, *421*, 129.
- [27] M. R. G. De Chailvo, R. C. Salvarezza, V. D. Moll, A. J. Arvia, *Electrochim. Acta.* **1985**, *30*, 1501.
- [28] D. Ben Hmamou, R. Salghi, A. Zarrok, B. Hammouti, S. S. Al-Deyab, Lh. Bazzi, H. Zarrouk, A. Chakir, B. Bammou, *Int. J. Electrochem. Sci.*, **2012**, *7*, 2361.
- [29] A. M. Amin, M. M. Ibrahim, *Corros. Sci.* **2011**, *53*, 873.
- [30] M. Lagrenée, B. Mernari, M. Bouanis, M. Traisnel, F. Bentiss, *Corros. Sci.* **2002**, *44*, 573.

- [31] G. K. Gomma, M. H. Wahdan, *Mater. Chem. Phys.* **1994**, 39, 142.
- [32] A. A. Nazeer, E. A. Ashour, N. K. Allam, *Mater. Chem. Phys.* **2014**, 144, 55.
- [33] N. Souissi, E. Triki, *Mater. Corros.* **2010**, 61, 695.
- [34] M. R. G. De Chialvo, M. F. L. De Mele, R. C. Salvarezza, A. J. Arvia, *Corros. Sci.* **1988**, 28, 121.
- [35] N. Saudi, A. Bellaouchou, A. Guenbour, A. Ben Bechir, E. M. Essassi, M. El Achouri, *Bull. Mater. Sci.* **2010**, 33, 313.

(Received: January 18, 2016)

W8856

(Accepted: February 21, 2016)